Hepatology Publish Ahead of Print
DOI:10.1097/HEP.0000000000000969

Reduction of Z alpha-1 antitrypsin polymers in human iPSC-Hepatocytes and mice by LRRK2 inhibitors

Authors: Deniz Kent[†,2,3], Soon Seng Ng[†,1], Adam M Syanda[†1], Payam Khoshkenar[3], Riccardo Ronzoni[4], Chao Zheng Li[2], Marina Zieger[3], Cindy Greer[3], Stephanie Hatch[6], Joe Segal[2], Samuel JI Blackford[1], Yu Ri Im[1], Vivek Chowdary[3], Taylor Ismali[5], Davide Danovi[2], Patrick A Lewis[7], James A Irving[4], Sunil Sahdeo[5], David A Lomas[4], Daniel Ebner[6], Christian Mueller[3] & S. Tamir Rashid*[,1]

Affiliations:
[1] Department of Metabolism, Digestion and Reproduction, Imperial College London, London W12 0NN, United Kingdom
[2] Centre for Stem Cells and Regenerative Medicine, King's College London, London SE1 9RT, United Kingdom
[3] Gene Therapy Center, University of Massachusetts, Worchester, Massachusetts 01655, United States
[4] UCL Respiratory and the Institute of Structural and Molecular Biology, University College London, London WC1E 6JF, United Kingdom
[5] Discovery Sciences, Janssen Research and Development, San Diego, California 92121, United States
[6] National Phenotypic Screening Centre, University of Oxford, Headington, Oxford OX3 7FZ, United Kingdom
[7] Royal Veterinary College, Royal College Street, London NW1 0TU, United Kingdom
[8] MRC London Institute of Medical Sciences, Du Cane Road, London W12 0NN, United Kingdom

[†]These authors contributed equally to this work

*Corresponding author.

Author contributions: Conceptualization: STR, CM, DK, SSN; Methodology: STR, SS, DE, RR, JAI, PK, DK, SSN, AMS, MZ, CG, SH, JS, SJIB, YRI, VC, TI, DD, PAL, SS ; Investigation: STR, CM; Visualization: DK, SSN, RR, AMS; Funding acquisition: STR, CM; Project administration: DK, SSN; Supervision: STR, CM, DD, DE, DAL; Writing – original draft: SSN, DK

Address for Correspondence: Email: t.rashid@imperial.ac.uk; Department of Metabolism, Digestion and Reproduction, Imperial College London, London W12 0NN, United Kingdom

Financial support and sponsorship: Alpha-1 Foundation

Conflicts of Interest:
Patrick A Lewis consults for Serna Bio. He received grants from LifeArc. Sunil Sahdeo is employed by and owns stock in Actio Biosciences. David A Lomas consults, received grants, and holds intellectual property rights with BioMarin. He has other interests with Grifols. Christian Mueller is employed by and owns stock in Sanofi. The remaining authors have no conflicts to report.

Keywords: iPSC, alpha-1 antitrypsin deficiency, LRRK2, small molecule screen, CZC-25146, protein misfolding, liver disease, novel therapeutic target, autophagy, PiZ.

List of abbreviations: A1AT: Alpha-1 antitrypsin; A1ATD: Alpha-1 antitrypsin deficiency; ALB: Albumin; ANOVA: Analysis of variance; ATG3: Autophagy-related protein 3; ATG5: Autophagy-related protein 5; ATZ: Alpha-1 antitrypsin Z variant polymer; BCA: Bicinchoninic acid; BSA: Bovine serum albumin; CHO-K1: Chinese hamster ovary cells, K1 line; DAPI: 4',6-diamidino-2-phenylindole; DMEM: Dulbecco's Modified Eagle Medium; DMSO: Dimethyl sulfoxide; ELISA: Enzyme-linked immunosorbent assay; ER: Endoplasmic reticulum; FBS: Foetal bovine serum; GAPDH: Glyceraldehyde 3-phosphate dehydrogenase; IFNγ: Interferon gamma; IL-1B: Interleukin 1 beta; IL-12p70: Interleukin 12 p70; IL-4: Interleukin 4; IL-6: Interleukin 6; iPSC: Induced pluripotent stem cell; iPSCs: Induced pluripotent stem cells; Ki67: Marker of proliferation Ki-67; LC3: Microtubule-associated protein 1A/1B-light chain 3; LC3-GFP: Microtubule-associated protein 1A/1B-light chain 3 fused to green fluorescent protein; LC3A: Light chain 3A; LC3B: Light chain 3B; LF-PVDF: Low-fluorescence polyvinylidene fluoride; LRRK2: Leucine-rich repeat kinase 2; NP40: Nonidet P-40 substitute; PBS: Phosphate-buffered saline; PASD: Periodic acid-Schiff diastase; PiZ: Z genetic variant; RPL13: Ribosomal protein L13; RT-qPCR: Quantitative reverse transcription polymerase chain reaction; SERPINA1: Serpin Family A Member 1; Tet-ON: Tetracycline-inducible system; TNFα: Tumour necrosis factor alpha; VPS34: Vacuolar protein sorting 34.

Graphical Abstract
GA1

Abstract: Alpha-1 antitrypsin deficiency (A1ATD) is a life-threatening condition caused by inheritance of the SERPINA1 'Z' genetic variant (PiZ) driving AAT protein misfolding in hepatocytes. There remain no approved medicines for this disease. Here, we report the results of a small molecule screen performed in patient derived iPSC-hepatocytes that identified Leucine-rich repeat kinase-2 (LRRK2) as a potentially new therapeutic target. Of the commercially available LRRK2 inhibitors tested, we identified CZC-25146, a candidate with favorable pharmacokinetic properties, as being capable of reducing polymer load, increasing normal AAT secretion, and reducing inflammatory cytokines in both cells and PiZ mice. Mechanistically, this effect was achieved through induction of autophagy. Our findings support the use of CZC-25146 and LRRK2 inhibitors in hepatic proteinopathy research and their further investigation as novel therapeutic candidates for A1ATD.

Introduction

The ability of a cell to tightly regulate protein quality is fundamental to life[1]. Failure can result in the accumulation of protein aggregates (proteinopathy) with devastating repercussions[2]. Accumulation of alpha-1 antitrypsin (AAT) protein aggregates is an archetypal example of how dysregulation in these mechanisms leads to life-threatening human disease[3–5]. In healthy individuals, AAT is a 52kDa glycoprotein product of the *SERPINA1* gene secreted from hepatocytes in the liver to the bloodstream, subsequently reaching the lungs, where it primarily acts as a neutrophil elastase inhibitor. The 'Z' variant describes a single base pair mutation in exon 5 of the *SERPINA1* gene which results in an amino acid substitution (lysine for glutamate) at position 342[5]. This substitution leads to structural changes in the hinge region of the AAT protein, altered folding dynamics, and predisposition to aggregation of retained polymeric protein (termed ATZ) within the endoplasmic reticulum (ER). Toxic accumulation of intra-hepatocytic ATZ, in turn, triggers inflammation, fibrosis, and downstream liver cancer and/or liver failure. In turn, lack of AAT reaching the lung leads to uninhibited neutrophil elastase-mediated parenchymal destruction and lung emphysema. Epidemiological studies suggest that there may be over 100,000 homozygous (ZZ) and over 100,000,000 heterozygous (MZ, SZ) patients suffering from associated liver disease globally[6]. Despite significant advances in our understanding of pathophysiology driven by ATZ accumulation, there remains no approved medicine to address this problem, with liver transplantation providing the only chance of cure. This represents a significant unmet medical need and requires urgent attention.

To address this challenge, we combined our prior expertise in chemical screening campaigns with our patient-derived induced pluripotent stem cell (iPSC)-hepatocyte expressing ATZ model[7–10] and screened a library of over 1,000 annotated small molecules known to effect protein trafficking pathways. Our objective was to identify ATZ polymer-lowering molecular targets. Hits from this initial screen were subsequently validated across additional patient-derived iPSC and cell models, before one candidate was taken forwards for further mechanistic and *in vivo* studies as described in the results sections below.

Materials and Methods

Cell lines

iPSCs: One in-house developed human iPSC line (line 1) and two gifted iPSC lines (line 2, PiZZ1, and line 3, PiZZ6 from Andrew Wilson Lab, Boston University) used in this study were reprogrammed from three homozygous PiZ patients (rs28929474) with severe liver disease. iPSCs were cultured in Essential 8 medium (Gibco) on Vitronectin (Sigma Aldrich) coated plates and passaged using ReLeSR (STEMCELL Technologies) every 3-4 days. iPSCs were differentiated into iPSC-hepatocytes using our previously established protocol[7]. In brief, iPSC-hepatocytes were differentiated until day 30 prior to use in all experiments, with plating into assay format taking place on day 21.

Tetracycline-inducible (Tet-ON) CHO-K1 cells expressing polymeric A1AT E324K (gift by Lomas Lab) were maintained as previously described[11]. CHO-K1 cells were co-treated using 1µg/mL doxycycline (Takara Bio Europe) and the small molecules for experiments described below.

LC3-GFP fibroblasts were gifted from the Carlton Lab (King's College London) and analyzed using both the Operetta CLS for quantitative assessment, and the SP8 confocal (Leica) for qualitative assessment. Fibroblasts were cultured in DMEM (Gibco) with 10% FBS (Sigma Aldrich) and 1% penicillin/streptomycin (Sigma Aldrich) and passaged once a week using trypsin (Sigma Aldrich). Fibroblasts used for experimentation were cultured in serum-free OptiMEM (ThermoFisher, 31985062).

Annotated compound screen

The National Phenotypic Screening Center conducted the annotated compound screen, using a compound library of known small molecules with annotated targets provided by Janssen Research and Development. One day before cell seeding, 384-well plates were coated with laminin-411 (LN411-03, BioLamina) at 3.75µg/cm^2. The PiZ and healthy control iPSC-hepatocytes used in the screen were commercially sourced

(Definigen), thawed in Def-HEP thawing media (Definigen), and plated at a density of 20,000 cells per well. Subsequently, the cells were maintained in Def-HEP Recovery & Maintenance Medium (Definigen) until day 13 post-seeding. JANUS G3 (Perkin Elmer) automated liquid handling system was used for media changes every two days until day 13, then for test compound dispensing. A library of 1,041 annotated small molecules were all dissolved in DMSO and tested at a final concentration of 10μM for each compound. The test compounds were left for 24 hours, with each compound being tested in duplicate in separate plates. Subsequently, the wells were washed, fixed with 4% paraformaldehyde, and permeabilized with 0.5% Triton X for 5 minutes. The samples were then blocked in 3% donkey serum in 1% BSA for 1 hour and incubated with primary antibodies at 4□C overnight. Polymeric alpha-1 antitrypsin (ATZ) was assessed using the 2C1 monoclonal antibody (1:250 dilution; gifted by the Lomas lab) and Alexa-488 donkey anti-mouse secondary antibody (1:500 dilution; A21202, Life Technologies). Image acquisition was performed on an In Cell 6000 Analyzer (Cytiva), and image analysis was performed with Columbus software (Perkin Elmer). The 2C1 signal was quantified by detection of the nuclei ($DAPI^+$ objects), then generating a ring-like structure by shape dilation by 2.5μm. The signal intensity was measured in the ring region to obtain the average polymer load measurement per cell in the well. An average of all cells per well was used in the downstream analyses and the fold-difference normalized to untreated PiZ cells and z-score calculation for each well. Albumin expression was assessed for quality control purposes and was measured using the anti-albumin goat monoclonal antibody (1:500 dilution; A80-129A, Bethyl) and Alexa-647 donkey anti-goat secondary antibody (1:500 dilution; A21447, Life Technologies). Compounds that led to cell death, as determined by a dramatic reduction in $DAPI^+$ objects or loss of albumin expression, were removed and excluded from the analysis. Compounds with a 2C1 Z-score in the vicinity of or lower than 1.92 (95^{th} percentile of healthy control cells) were defined as hits and selected for a confirmatory screen. Fourteen hits identified in the primary screen were confirmed in an independent experimental repeat. LRRK2 was subsequently selected for further investigation.

Validation of compound screen

CZC-25146 (Tocris, 6071), CZC-542525 (Sigma, S6534), MLi-2 (Sigma, S9694), GNE-9605 (Sigma, S7368), GNE-0877 (Sigma, S7367) and GNE-7915 (Sigma, S7528) were tested on day 30 PiZ iPSC-hepatocytes for either 24 or 48 hours. Polymeric ATZ was assessed using the polymer-specific antibody 2C1 (gifted by the Lomas Lab) and viability was assessed using the Presto Blue Viability Assay (ThermoFisher) conducted according to manufacturer's instructions. The appropriate dose-response starting point for each compound was determined using the manufacturer's solubility data and by calculating the highest compound concentration that could be used without exceeding 0.1% DMSO in the culture. Antibodies used include: LRRK2 (Abcam, ab133474), total hA1AT (Abcam, ab9373), human ALB (Bethyl Laboratories, A80-129A). AAT ELISA (Abcam, ab108798) was used according to the manufacturer's instructions. High-content imaging was conducted using the Operetta CLS (Perkin Elmer) and data was analyzed using Harmony software (Perkin Elmer). Differential gene expression was detected using quantitative reverse transcription polymerase chain reaction (RT-qPCR). The qPCR was then performed on the CFX Connect Real-Time PCR Detection System (BioRad), with all data normalised to GAPDH and RPL13 housekeeping genes. Primer sequences are listed in Table S1, http://links.lww.com/HEP/I543. The immunoblotting analysis on the ATZ polymer expression in cells were prepared as previously reported [(12)]. In brief, 1%NP40-soluble and -insoluble fractions were immunoprecipitated using the 2C1 antibody [(13)]. Samples were resolved on pre-cast NuPAGE™ 4–12% w/v acrylamide Bis/Tris Protein Gels (Invitrogen, ThermoFisher Scientific Ltd., Loughborough, UK) and transferred to LF-PVDF membranes (Millipore Ltd., Hertfordshire, UK). Membranes were saturated in 5% w/v low-fat milk (Cell Signaling Technology, Danvers, MA, USA) in PBS-0.1% v/v Tween, probed with anti-human AAT polyclonal antibody (Dako, Agilent, Stockport, UK) followed by fluorescent goat anti-rabbit 488 secondary antibodies (Santa Cruz Biotechnology, Dallas, TX, USA), acquired with an iBright1500 (GE Healthcare Life Sciences, Amersham, UK), and analyzed using Image Studio Lite software (LI-COR Biosciences, Cambridge, UK). The pulse chase experiments were performed as previously described [(14)].

Pre-clinical mouse study

The PiZ mouse model used in our proof-of-concept study is a transgenic model that carries the PiZ variant of the human A1AT gene. This causes human ATZ accumulation within the ER of hepatocytes and consequent liver injury, mirroring the pathology observed in human patients[15]. Sample sizes were chosen based on result variability, necessary statistical power, and the ethical need to minimize animal use. Only male mice were used in the study to remove sex-associated confounders. Male PiZ mice have been reported to prone to a more severe and reproducible ATZ phenotype[16]. Endpoints for experiments with mice adhered to institutionally approved criteria. Blinding was not applied. The number of replicates varied across experiments, as detailed in the respective figure legends. The mice were randomized into experimental groups at 6 weeks and administered with CZC-25146 at 250mg/kg dissolved in pure DMSO for 14 consecutive days by oral gavage. Mice were subsequently culled and each lobe of the liver was separated independently. For immunohistochemistry experiments, all samples were washed thrice with PBS, followed by a 24-hour fixation with 10% formalin. Samples were then rewashed thrice with PBS, before being processed, embedded into paraffin, sliced, and stained. The antibodies/stains used were: PASD (Sigma Aldrich, 395B-1KT), LC3 (Abcam, ab48394), Ki67 (Abcam, ab15580). *In vivo* image analysis was conducted by taking three images of each liver lobe at 5x magnification, equally distributed across each lobe (15 images per mouse). The images were analyzed using ImageJ. Western Blot analysis was prepared by homogenizing the frozen liver tissue in Cell Lysis Buffer (Cell Signaling Technology, 9803) supplemented with phosphatase inhibitor (#78427, ThermoFisher) and protease inhibitor (ThermoFisher, 78429) using TissueLyzer II (Qiagen) for 30 minutes. Protein concentrations were normalized using a Pierce™ BCA protein assay kit (ThermoFisher) according to the manufacturer's instructions. Processed proteins samples were run on 3–8% NuPAGE Tris-Acetate 1.5mM pre-cast gels (ThermoFisher, EA0378BOX) and primary antibodies used were anti-phospho-Ser935 LRRK2 [UDD2 10(12)] (Abcam, ab133450) or anti-LRRK2 [MJFF2] (Abcam, ab133474). The secondary antibody was IR Dye 680RD (Licor, 962-68073). Blots were imaged using ChemiDoc MP (Biorad). Quantitation of the bands was performed using Image Studio (Licor). All animal experiments were performed in accordance with UK Home Office regulations (UK Home Office Project License number PPL P26C63193).

Quantification and statistical analysis

Statistical analysis involved a Kolmogorov-Smirnov test for normality, followed by an analysis of variance. When more than two groups were compared, the normality and variance analysis was followed by either an Ordinary One-way ANOVA (for parametric datasets) or Kruskal-Wallis test (for non-parametric datasets), followed by a Dunn's (non-parametric) or Dunnett's (parametric) multiple comparison test. If two groups were compared, the normality and variance testing was followed by either a T-test (parametric data) or a Mann-Whitney Test (non-parametric data). *=p<0.05, **=p<0.01, ***=p<0.001, ****=p<0.0001. All statistics were performed using GraphPad Prism.

Results

A high-throughput annotated screen identifies new targets for A1ATD

The goal of this study was to identify new therapeutics for patients with alpha-1 antitrypsin deficiency (A1ATD). To this end, we hypothesized that compounds known to target protein degradation and ER stress would cause a reduction of alpha-1 polymer (ATZ) load in hepatocytes[4,17,18]. Accordingly, an annotated compound library containing molecules specific to these pathways was screened against our previously developed *in vitro* iPSC disease model derived from a patient who suffered from A1ATD-related liver disease as a result of carrying the Z genetic mutation (PiZ, Figure 1A)[7,10]. The iPSC-hepatocyte model was miniaturized into a 384-well plate format, with high ATZ polymer (2C1 antibody) and albumin expression representing the disease and hepatic phenotypes, respectively (Figure S1A, http://links.lww.com/HEP/I544). The screen was designed to identify compounds capable of reducing ATZ polymer (represented as Z-score) whilst preserving cell viability and phenotype. We tested each compound at 10μM concentration in duplicate for 24 hours. Efficacy was interpreted as a reduction in immunofluorescence intensity following staining with the ATZ polymer-specific monoclonal antibody (2C1)[13] and captured using high-throughput confocal imaging. The analysis pipeline involved automatic

nucleus detection and counting by DAPI signal for ATZ polymer quantification (Figure 1B). In brief, for every detected DAPI+ object (nucleus), a ring mask with a 2.5μm width was created surrounding it. The ATZ signal intensity was then quantified within the bounds of the ring mask and assigned a z-score. Of the 1,041 compounds screened, 14 compounds demonstrated significantly decreased ATZ expression z-scores (<-1.92) (Figure 1C and S1B), to within the range of healthy control (Figure S1C, http://links.lww.com/HEP/I544). Given its relevance to other proteostatic disorders such as Parkinson's disease, one of the targets identified, LRRK2, was selected for further validation (Figure 1D).

LRRK2 inhibitors reduce ATZ polymers in iPSC and CHO disease models

Our working hypothesis was that LRRK2 regulates ATZ polymer load and accordingly represented a potentially novel therapeutic target. We therefore tested the polymer-reducing effect of commercially available LRRK2 inhibitors (10μM) whose chemical structures target different binding sites of the LRRK2 protein. In patient-derived iPSC-hepatocytes, we observed significant polymer reduction and retained cell viability with all but one compound (Figure 2A-B). Then, using the Tet-ON CHO model (genetically modified Chinese Hamster Ovary cells expressing mutant Z human AAT protein upon tetracycline induction [(11)]) we confirmed polymer reduction occurred in a dose-dependent manner (Figure 2C).

CZC-25146 reduces polymer load whilst restoring secretion of normal AAT in iPSC-hepatocytes

One of the LRRK2 inhibitors tested, CZC-25146 (CZC), had previously been reported to have poor blood-brain barrier penetrance [(19)]. This, along with its promising polymer reduction and viability profile across the different cell models tested, suggested it would represent the most favorable compound for targeting LRRK2 in the liver. This compound was therefore taken forward for subsequent investigations. We first showed that 24-hour treatment with CZC-25146 generated a dose-dependent reduction of ATZ polymer load across three different iPSC-hepatocyte lines (three different patient donors) without compromising cell viability nor total AAT protein expression (Figure 3A-B, Figure S2, http://links.lww.com/HEP/I544). We validated polymer decrease (Figure 3C) and no change in intracellular AAT (Figure 3D) in independent immunofluorescence experiments across all three lines. We previously showed analysis of soluble and insoluble intracellular ATZ fractions provided important information on the kinetics of polymer accumulation and degradation[(20)]. Accordingly, we profiled the intracellular soluble and insoluble fractions of polymeric ATZ following LRRK2 inhibitor treatment as before. In brief, we lysed the cells treated with CZC-25146 using 1% NP40 and performed immunoprecipitation using the polymer-specific monoclonal antibody 2C1. Immunoblotting assays demonstrated a dose-dependent reduction in intracellular ATZ polymer, in both soluble and insoluble fractions (Figure 3E). Notably, overall secretion of AAT into the cell culture medium was also found to be significantly increased (Figure 3F). These findings have direct translational relevance since they support the idea of a single agent such as CZC-25146, being able to treat both lung (deficiency of normal AAT) and liver (toxicity of ATZ polymer accumulation) pathologies at the same time.

CZC-25146 reduces polymer load and inflammation in mice

To interrogate the potential of CZC-25146 as a therapeutic for patients, we conducted a proof-of-concept study using the PiZ mouse model[(15)]. The PiZ mice used in our studies were genetically modified to accumulate human ATZ protein in the ER of murine hepatocytes in a manner analogous to the pathology observed in patients. Notably though, this animal model does not suffer from deficiency of circulating AAT due to endogenous production of murine AAT and so does not model the lung pathology aspect of the disease. Nonetheless, it is a suitable animal model to study the impact of CZC-25146 on liver pathology. Mice were dosed with 250mg/kg CZC-25146 (or vehicle control) via oral gavage for 14 days. We chose male mice aged six weeks for our study since this age is thought to coincide with peak polymer accumulation levels in this model [(21)]. At a dosage of 250mg/kg, CZC-25146 reduced polymer levels, as evaluated by density of PAS-positive, diastase-resistant (PASD) globules, in all mice (Figure 4A). Examination under higher magnification revealed the histological PASD reduction profile to be consistent across all five liver lobes (Figure 4B, top). Overall, globule levels were reduced from 60% in vehicle-

treated controls to 37% in the CZC-25146 treated group (Figure 4B, bottom). Immunoblotting of immunoprecipitated polymers retrieved from the livers confirmed the observed reduction in PAS staining was due to reduction in ATZ polymer (Figure 4C). In parallel, we detected a greater than two-fold increase in serum levels of total human AAT (Figure 4D) and 1.7-fold increase in serum levels of polymeric ATZ (Figure 4E) after treatment. Next, using the MesoScale Discovery inflammatory cytokine array, we found that CZC-25146 administration led to a decrease in inflammatory cytokines, specifically IL-1B, IL-12p70, IFNγ, IL-4, TNFα, and IL-6 (Figure 4F), underlining the direct anti-inflammatory potency of the drug or decrease of inflammation upon hepatocyte polymeric load reduction. From a safety standpoint, no apparent drug-induced liver injury was observed after treatment, with the liver architecture remaining intact throughout, no significant weight changes (Figure S3A-B, http://links.lww.com/HEP/I545) and hepatocytes not demonstrating hyperproliferation (Ki67) or carcinogenesis (Figure S3C-D top and middle, http://links.lww.com/HEP/I545). Lastly, although CZC-25146 is reported to be a highly selective LRRK2 kinase inhibitor, activity against other kinases (PLK4, GAK, TNK1, CAMKK2, and PIP4K2C) has also been reported [19]. To confirm that the polymer reduction observed following CZC-25146 treatment of PiZ mice was a consequence of LRRK2 kinase inhibition, we harvested livers and purified both mRNA and protein for RT-qPCR and immunoblotting analysis. *LRRK2* transcriptional (Figure 4G) and protein expression levels (Figure 4H) remained unchanged following treatment, though LRRK2 activity, as measured by autophosphorylation represented by pSer935-LRRK2, was reduced significantly.

Profiling of CZC-25146-mediated polymer reduction dynamics using pulse-chase

To explore the kinetics of ATZ reduction following CZC-25146 treatment, we performed pulse-chase experiments on inducible Tet-ON CHO-K1 cells expressing ATZ (Figure 5A) as per our previous work[11,14,20,22–25]. We used radioactive ^{35}S-Met/Cys for labelling and chased at 1, 4, and 8 hours. The separation of polymeric ATZ into soluble and insoluble fractions, coupled with the collection of culture media representing the extracellular fraction, allowed us to track ATZ polymer kinetics (Figure 5B). Both the control and treatment groups demonstrated formation of ATZ polymer over time, indicating that the kinetic of AAT production was preserved in both groups. However, the kinetic of ATZ polymer formation was delayed upon CZC-25146 treatment in the insoluble fraction. Notably, the treated cells also demonstrated marked ATZ polymer reduction in both the soluble and insoluble fractions. Coupling these observations with the negligible impact on the secreted ATZ seen in the extracellular fraction, we hypothesize that CZC-25146-induced polymer load reduction is driven by intracellular degradative mechanisms.

CZC-25146-mediated polymer reduction is associated with autophagy induction

Dysregulated intracellular protein degradation pathways have been postulated to contribute to the liver disease associated with ATZ polymer formation[4]. Degradation by autophagic mechanisms has gained particular interest in the field since deletion of the *Atg5* gene was shown to exacerbate ATZ polymer load accumulation in the ER lumen[26]. As LRRK2 is reported to be a regulator of autophagy[27–29], we hypothesized that the mechanism of CZC-25146 ATZ polymer reduction could be via induction of autophagy. To test our hypothesis, we first validated the functional link between CZC-25146 and autophagy. Using the LC3-GFP human fibroblast line, in which the autophagosome membrane is labelled with GFP, we found that CZC-25146-induced autophagosome formation (LC3-GFP immunofluorescence) occurred at levels similar to that observed with Rapamycin, which is known to be a potent inducer of autophagy (Figure 6A)[30]. Time-course analysis revealed that autophagosome formation peaked at 2 hours post-exposure to both CZC-25146 and Rapamycin, before gradually decreasing (Figure 6B). After establishing the link between CZC-25146 and enhanced autophagosome formation in fibroblasts, we evaluated the expression of autophagy genes in CZC-25146-treated PiZ patient-derived iPSC-hepatocytes. *VPS34,* which is critical for the initiation of autophagy, and downstream *ATG*-related genes such as *ATG3*, *ATG5*, *Calnexin*, *LC3A* and *LC3B* were all found to be significantly upregulated in a dose-responsive manner following treatment (Figure 6C & Figure S4, http://links.lww.com/HEP/I546). Subsequently, we used the LC3-II to LC3-I ratio (as detected by immunoblotting) as a measure of autophagic flux and found

that it increased in response to treatment with CZC-25146 (or rapamycin) (Figure 6D). Therefore, we hypothesize that CZC-25146 both increases autophagosome formation and reduces ATZ polymer load, which in turn supports a link between the two mechanisms. To investigate whether the accumulation of autophagosomes was driven by induction of autophagy, rather than the impairment of autolysosomal fusion and hence the degradation of autophagosomes, we performed the autophagic flux assay in the presence of a lysosomal acidification inhibitor, bafilomycin A (Figure 6E)[31]. As expected, LC3-II expression of cells treated with CZC-25146 was increased in a dose-dependent manner, and the presence of bafilomycin A increased the LC3-II level even further compared to both vehicle control and treatment with CZC-25146 alone. This indicated that the reduction of ATZ polymer load observed following the CZC-25146 treatment was driven by autophagy induction, rather than reduced LC3 recycling. To demonstrate the functional importance of this observation, we then treated cells with a combination of ammonium chloride, NH_4Cl, an autophagy inhibitor[32] and CZC-25146. As expected, we found NH_4Cl partially reversed the polymer-lowering effect of CZC-25146 (Figure 6F). Finally, to validate CZC-25146 had the same effect *in vivo,* we performed immunohistochemistry for LC3 on treated PiZ mice. These analyses confirmed administration of CZC-25146 restored autophagy to levels seen in healthy controls (Figure 6G-H, S5).

Discussion

Using a patient derived iPSC-hepatocyte model of PiZ alpha-1 antitrypsin deficiency, we screened over 1,000 annotated small molecules for their ability to reduce ATZ polymer load. Based on the initial screening and its clinical relevance in other protein misfolding diseases, LRRK2 was selected for further investigation. We then demonstrated that a small library of commercially available LRRK2 inhibitors reduced ATZ polymer levels across both iPSC and CHO-K1 cell models in a dose dependent manner. Some variation in sensitivity to the compounds was noted, likely attributed to different genetic backgrounds of the cell lines. Among these inhibitors, CZC-25146, was also found to reduce polymer load and inflammation in PiZ mice whilst increasing secretion of AAT. Finally, we confirmed the mechanism of action of CZC-25146 to be via inhibition of LRRK2 kinase activity and induction of autophagy. Cumulatively, our data provide evidence that LRRK2 inhibitors promote autophagic clearance of ATZ polymers from hepatocytes, and that CZC-25146, along with related LRRK2 inhibitors, may represent new therapeutic approaches for patients with alpha-1-antitrypsin deficiency.

PiZ-associated liver disease arises by gain-of-function toxicity due to ATZ polymer accumulation in hepatocytes. PiZ-associated lung disease results from parenchymal degradation secondary to insufficient AAT levels. Replacement of missing AAT via donor plasma infusions is available clinically and has shown potential benefits in halting progression of the lung disease[33,34]. Recent approaches to suppress ATZ production in the liver using RNA interference (RNAi) have shown very promising results in clinical trials[35,36]. However, on their own neither AAT supplementation nor RNAi are expected to provide a definitive 'cure' for patients as they cannot concurrently address both liver and lung pathologies at the same time. Whilst gene editing to correct underlying mutations in the *SERPINA1* gene or cell therapy [8] could achieve this, there are currently no technologies advanced enough to facilitate sufficient levels of genetic correction or cellular engraftment to yield clinically relevant outcomes. In the interim, a small molecule approach to either block polymer formation[14] or increase polymer degradation (NCT05643495) represent two promising alternative solutions, which may be complementary. Targeting degradation pathways, such as autophagy, are especially attractive since they could rationally address the wide clinical phenotype spectrum observed in individuals with the same *SERPINA1* genetic mutation, hypothesized by many to be due to varied protein degradation potencies.

Autophagy has already been reported to potentially play an important role in ATZ polymer degradation, even though the specific molecular players involved have remained elusive[37]. This may partially explain why attempts to augment autophagic flux in a non-specific manner have so far not yielded clinical success (NCT01379469)[18]. Identifying hepatocyte-specific targets to accelerate polymer destruction and maintain or restore normal AAT production may circumvent this issue. We believe that identifying these molecular targets has been impeded by use of non-human disease models (i.e. models expressing mutant human

SERPINA1 in non-human backgrounds such as mouse, hamster or worms[38]. To address this limitation, we therefore performed our small molecule screen in iPSC-hepatocytes derived from patients with clinically documented ATZ polymer-associated disease. Thus, both the genetic defect (Glu-Lys 342) and protein degradation mechanisms were reproduced in our model in a patient-specific manner. This technology accordingly has enabled us to identify molecular targets that, to the best of our knowledge, could be amenable to intervention in liver proteinopathies.

Of the hits from our screen, we chose to focus on LRRK2, a seven-domain, 285kDa cytosolic protein implicated in lysosomal degradation[39,40]. The rationale for focusing on LRRK2 was several-fold. Firstly, previous research by our group, and others, suggested that patients harboring mutant AAT develop liver disease when their polymer disposal mechanisms, specifically the autophagy-lysosomal-degradation pathway (ALP), become overwhelmed. LRRK2, therefore, could represent a critical but hitherto unrecognized regulator of hepatocyte ALP. Consistent with this, we found that inhibition of LRRK2 kinase activity was sufficient to decrease ATZ polymer disposal and ameliorate the associated liver disease. Secondly, a number of genetic variants at the *LRRK2* locus have been identified as key contributors in another protein misfolding disorder, Parkinson's disease (PD)[40]. This association has prompted the development of LRRK2 kinase inhibitors and antisense oligonucleotides as potential new medicines for PD, with leading candidates expected to enter late-stage clinical trials this year[41]. The precise understanding of how LRRK2 inhibitors regulate protein disposal remains incomplete. Several studies suggest LRRK2 acts at different stages of the ALP, although the results are conflicting in terms of the mediation process and the net physiological direction. For example, in neurons derived from patients with PD, it has been shown that Rab10, a mediator of LRRK2 kinase activity, negatively regulates lysosomal activity and clearance of alpha-synuclein[42].
Conversely, in infected macrophages, this regulation is achieved via a Rab8A- CHMP4B axis[43]. In contrast, LRRK2 overexpression in kidney and neuroendocrine cells induced autophagy through a Ca^{2+}/CaMKK/AMPK pathway[44]. These studies support a paradigm whereby the role of LRRK2 in ALP is both cell- and disease-specific. Our data suggests the level of LRRK2 kinase activity is an important regulator of ATZ polymer handling via the ALP in hepatocytes, implying that a targeted intervention on LRRK2 could lead to a therapeutic reduction in polymer load and subsequent reversal of liver disease in A1ATD. At this time, however, the specific molecular players interacting with LRRK2 to achieve this are yet to be elucidated. To this end, future studies should endeavor not only to identify these elements but also consider a more comprehensive analysis of the effects of long-term LRRK2 inhibition on the amelioration of liver fibrosis. Notably, such knowledge may also improve our understanding of the pathological mechanisms in other liver diseases such as alcoholic (ALD) and non-alcoholic fatty liver disease (NAFLD), where protein aggregates and ER stress are postulated to represent fundamental components of the pathology[45–49].

Collectively, our data advocate for further investigation of the potential therapeutic role of CZC-25146 in A1ATD. This compound, initially developed as a treatment for Parkinson's disease, did not advance in clinical development due to its limited ability to cross the blood-brain barrier[19]. In contrast to its original indication, such a pharmacokinetic profile may prove beneficial when targeting liver pathologies. More broadly, we propose LRRK2 inhibitors, especially those already shown to be safe in clinical trials[27], be considered to not only help further our mechanistic understanding of A1ATD biology in the laboratory, but also for therapeutic use in clinic.

Acknowledgements

We would like to thank Prof Fiona Watt and Dr Benedict Oules for the reagents and support.
The authors acknowledge the funding from the Alpha-1 Foundation to support this work. We would also like to thank the NIHR Guy's and St Thomas's Biomedical Research Centre, and the NIHR Imperial BRC iPSC and Organoid Core Facility, Imperial College London, UK.

Declaration of interests

The authors declare no conflicts of interest relevant to the study presented here.

References

1. Chen B, Retzlaff M, Roos T, Frydman J. Cellular strategies of protein quality control. Cold Spring Harb. Perspect. Biol. 2011;3:1–14.
2. Hartl FU. Protein misfolding diseases. Annu. Rev. Biochem. 2017;86:21–26.
3. Pan S, Huang L, McPherson J, Muzny D, Rouhani F, et al. Single nucleotide polymorphism-mediated translational suppression of endoplasmic reticulum mannosidase I modifies the onset of end-stage liver disease in alpha1-antitrypsin deficiency. Hepatology. 2009;50:275–281.
4. Wu Y, Whitman I, Molmenti E, Moore K, Hippenmeyer P, et al. A lag in intracellular degradation of mutant α1-antitrypsin correlates with the liver disease phenotype in homozygous PiZZ α1-antitrypsin deficiency. Proc. Natl. Acad. Sci. U. S. A. 1994;91:9014–9018.
5. Lomas DA, Evans DL, Finch JT, Carrell RW. The mechanism of Z α1-antitrypsin accumulation in the liver. Nature. 1992;357:605–607.
6. Nakanishi T, Forgetta V, Handa T, Hirai T, Mooser V, et al. The undiagnosed disease burden associated with alpha-1 antitrypsin deficiency genotypes. Eur. Respir. J. 2020;56.
7. Rashid ST, Corbineau S, Hannan N, Marciniak SJ, Miranda E, et al. Modeling inherited metabolic disorders of the liver using human induced pluripotent stem cells. J. Clin. Invest. 2010;120:3127–3136.
8. Yusa K, Rashid ST, Strick-Marchand H, Varela I, Liu PQ, et al. Targeted gene correction of α1-antitrypsin deficiency in induced pluripotent stem cells. Nature. 2011;478:391–394.
9. Ong J, Serra MP, Segal J, Cujba AM, Ng SS, et al. Imaging-Based Screen Identifies Laminin 411 as a Physiologically Relevant Niche Factor with Importance for i-Hep Applications. Stem Cell Reports. 2018;10:693–702.
10. Ng SS, Saeb-Parsy K, Blackford SJI, Segal JM, Serra MP, et al. Human iPS derived progenitors bioengineered into liver organoids using an inverted colloidal crystal poly (ethylene glycol) scaffold. Biomaterials. 2018;182:299–311.
11. Ordóñez A, Snapp EL, Tan L, Miranda E, Marciniak SJ, et al. Endoplasmic reticulum polymers impair luminal protein mobility and sensitize to cellular stress in alpha1-antitrypsin deficiency. Hepatology. 2013;57:2049–2060.
12. Ronzoni R, Ferrarotti I, D'acunto E, Balderacchi AM, Ottaviani S, et al. The importance of n186 in the alpha-1-antitrypsin shutter region is revealed by the novel bologna deficiency variant. Int. J. Mol. Sci. 2021;22.
13. Miranda E, Pérez J, Ekeowa UI, Hadzic N, Kalsheker N, et al. A novel monoclonal antibody to characterize pathogenic polymers in liver disease associated with α1-antitrypsin deficiency. Hepatology. 2010;52:1078–1088.
14. Lomas DA, Irving JA, Arico-Muendel C, Belyanskaya S, Brewster A, et al. Development of a small molecule that corrects misfolding and increases secretion of Z α 1 -antitrypsin . EMBO Mol. Med. 2021;13:e13167.
15. Carlson JA, Barton Rogers B, Sifers RN, Finegold MJ, Clift SM, et al. Accumulation of PiZ α1-antitrypsin causes liver damage in transgenic mice. J. Clin. Invest. 1989;83:1183–1190.
16. Rudnick DA, Liao Y, An JK, Muglia LJ, Perlmutter DH, et al. Analyses of Hepatocellular Proliferation in a Mouse Model of α-1-Antitrypsin Deficiency. Hepatology. 2004;39:1048–1055.
17. Lin L, Schmidt B, Teckman J, Perlmutter DH. A Naturally Occurring Nonpolymerogenic Mutant of α1-Antitrypsin Characterized by Prolonged Retention in the Endoplasmic Reticulum. J. Biol. Chem. 2001;276:33893–33898.
18. Hidvegi T, Ewing M, Hale P, Dippold C, Beckett C, et al. An autophagy-enhancing drug promotes degradation of mutant α1-antitrypsin Z and reduces hepatic fibrosis. Science (80-.). 2010;329:229–232.
19. Ramsden N, Perrin J, Ren Z, Lee BD, Zinn N, et al. Chemoproteomics-based design of potent LRRK2-selective lead compounds that attenuate Parkinson's disease-related toxicity in human neurons. ACS Chem. Biol. 2011;6:1021–1028.

20. Ronzoni R, Heyer-Chauhan N, Fra A, Pearce AC, Rüdiger M, et al. The molecular species responsible for α1-antitrypsin deficiency are suppressed by a small molecule chaperone. FEBS J. 2021;288:2222–2237.
21. Borel F, Tang Q, Gernoux G, Greer C, Wang Z, et al. Survival Advantage of Both Human Hepatocyte Xenografts and Genome-Edited Hepatocytes for Treatment of α-1 Antitrypsin Deficiency. Mol. Ther. 2017;25:2477–2489.
22. Segeritz CP, Rashid ST, de Brito MC, Serra MP, Ordonez A, et al. hiPSC hepatocyte model demonstrates the role of unfolded protein response and inflammatory networks in α1-antitrypsin deficiency. J. Hepatol. 2018;69:851–860.
23. Malintan NT, Buckingham SD, Lomas DA, Sattelle DB. Calcium signalling in mammalian cell lines expressing wild type and mutant human α1-Antitrypsin. Sci. Rep. 2019;9:17293.
24. Tan L, Dickens JA, DeMeo DL, Miranda E, Perez J, et al. Circulating polymers in α1-antitrypsin deficiency. Eur. Respir. J. 2014;43:1501–1504.
25. Miranda E, Römisch K, Lomas DA. Mutants of neuroserpin that cause dementia accumulate as polymers within the endoplasmic reticulum. J. Biol. Chem. 2004;279:28283–28291.
26. Kamimoto T, Shoji S, Hidvegi T, Mizushima N, Umebayashi K, et al. Intracellular inclusions containing mutant α1-antitrypsin Z are propagated in the absence of autophagic activity. J. Biol. Chem. 2006;281:4467–4476.
27. West AB. Achieving neuroprotection with LRRK2 kinase inhibitors in Parkinson disease. Exp. Neurol. 2017;298:236–245.
28. Christensen K V., Smith GP, Williamson DS. Development of LRRK2 Inhibitors for the Treatment of Parkinson's Disease. Prog. Med. Chem. 2017;56:37–80.
29. Li T, Yang D, Zhong S, Thomas JM, Xue F, et al. Novel LRRK2 GTP-binding inhibitors reduced degeneration in Parkinson's disease cell and mouse models. Hum. Mol. Genet. 2014;23:6212–6222.
30. Kaushal S, Annamali M, Blomenkamp K, Rudnick D, Halloran D, et al. Rapamycin reduces intrahepatic alpha-1-antitrypsin mutant Z protein polymers and liver injury in a mouse model. Exp. Biol. Med. 2010;235:700–709.
31. Manzoni C, Mamais A, Dihanich S, Abeti R, Soutar MPM, et al. Inhibition of LRRK2 kinase activity stimulates macroautophagy. Biochim. Biophys. Acta - Mol. Cell Res. 2013;1833:2900–2910.
32. Kaushik S, Massey AC, Mizushima N, Cuervo AM. Constitutive activation of chaperone-mediated autophagy in cells with impaired macroautophagy. Mol. Biol. Cell. 2008;19:2179–2192.
33. McElvaney NG, Burdon J, Holmes M, Glanville A, Wark PAB, et al. Long-term efficacy and safety of α1 proteinase inhibitor treatment for emphysema caused by severe α1 antitrypsin deficiency: an open-label extension trial (RAPID-OLE). Lancet Respir. Med. 2017;5:51–60.
34. Chapman KR, Burdon JGW, Piitulainen E, Sandhaus RA, Seersholm N, et al. Intravenous augmentation treatment and lung density in severe α1 antitrypsin deficiency (RAPID): A randomised, double-blind, placebo-controlled trial. Lancet. 2015;386:360–368.
35. Turner AM, Stolk J, Bals R, Lickliter JD, Hamilton J, et al. Hepatic-targeted RNA interference provides robust and persistent knockdown of alpha-1 antitrypsin levels in ZZ patients. J. Hepatol. 2018;69:378–384.
36. Strnad P, Mandorfer M, Choudhury G, Griffiths W, Trautwein C, et al. Fazirsiran for Liver Disease Associated with Alpha1-Antitrypsin Deficiency _ Enhanced Reader.pdf. N. Engl. J. Med. 2022;387:514–524.
37. Fregno I, Molinari M. Proteasomal and lysosomal clearance of faulty secretory proteins: ER-associated degradation (ERAD) and ER-to-lysosome-associated degradation (ERLAD) pathways. Crit. Rev. Biochem. Mol. Biol. 2019;54:153–163.
38. Hidvegi T, Schmidt BZ, Hale P, Perlmutter DH. Accumulation of mutant α1-antitrypsin Z in the endoplasmic reticulum activities caspases-4 and -12, NFκB, and BAP31 but not the unfolded protein response. J. Biol. Chem. 2005;280:39002–39015.
39. Obergasteiger J, Frapporti G, Lamonaca G, Pizzi S, Picard A, et al. Kinase inhibition of G2019S-LRRK2 enhances autolysosome formation and function to reduce endogenous alpha-synuclein

intracellular inclusions. Cell Death Discov. 2020;6:45.
40. Esteves AR, Swerdlow RH, Cardoso SM. LRRK2, a puzzling protein: Insights into Parkinson's disease pathogenesis. Exp. Neurol. 2014;261:206–216.
41. Schneider SA, Hizli B, Alcalay RN. Emerging Targeted Therapeutics for Genetic Subtypes of Parkinsonism. Neurotherapeutics. 2020;17:1378–1392.
42. Ysselstein D, Nguyen M, Young TJ, Severino A, Schwake M, et al. LRRK2 kinase activity regulates lysosomal glucocerebrosidase in neurons derived from Parkinson's disease patients. Nat. Commun. 2019;10:5570.
43. Herbst S, Campbell P, Harvey J, Bernard EM, Papayannopoulos V, et al. LRRK 2 activation controls the repair of damaged endomembranes in macrophages . EMBO J. 2020;39:e104494.
44. Gómez-Suaga P, Luzón-Toro B, Churamani D, Zhang L, Bloor-Young D, et al. Leucine-rich repeat kinase 2 regulates autophagy through a calcium-dependent pathway involving NAADP. Hum. Mol. Genet. 2012;21:511–525.
45. Lebeaupin C, Vallée D, Hazari Y, Hetz C, Chevet E, et al. Endoplasmic reticulum stress signalling and the pathogenesis of non-alcoholic fatty liver disease. J. Hepatol. 2018;69:927–947.
46. Dara L, Ji C, Kaplowitz N. The contribution of endoplasmic reticulum stress to liver diseases. Hepatology. 2011;53:1752–1763.
47. Strnad P, Nuraldeen R, Guldiken N, Hartmann D, Mahajan V, et al. Broad spectrum of hepatocyte inclusions in humans, animals, and experimental models. Compr. Physiol. 2013;3:1393–1436.
48. Strnad P, Buch S, Hamesch K, Fischer J, Rosendahl J, et al. Heterozygous carriage of the alpha1-antitrypsin Pi∗Z variant increases the risk to develop liver cirrhosis. Gut. 2019;68:1099–1107.
49. Belorgey D, Hägglöf P, Karlsson-Li S, Lomas DA. Protein misfolding and the serpinopathies. Prion. 2007;1:15–20.

Figure 1: A high-throughput annotated compound screen in patient-derived iPSC-hepatocytes identifies new targets for reducing alpha-1 antitrypsin Z (ATZ) polymers. (A) Schematic of the overall approach. (B) Image analysis pipeline involved nucleus detection and counting by DAPI signal. Each detected DAPI+ object was used to draw a 2.5um ring mask for quantification of 2C1 signal (polymeric ATZ) in each cell. (C) Average polymer signal/cell was recorded and plotted following addition of each compound in triplicate. Reduction in polymer load (2C1) was used as a marker of therapeutic efficacy. Compounds with Z-score lower than -1.92 (95th percentile of healthy control cells) were selected for follow up (shown in green). Untreated PiZ cells shown in black. Each dot represents the average of two measurements taken for each compound. N=1,041. (D) ID 22380519 targeting LRRK2 was identified as the top hit following the initial screen and the confirmatory dose-dependent study. A dose-dependent response was observed - polymer reduction (efficacy) in pink and live cells (viability) shown in black, indicating no severe cytotoxic effects. Both readouts were quantified using immunofluorescence. Data are represented as mean ± SD.

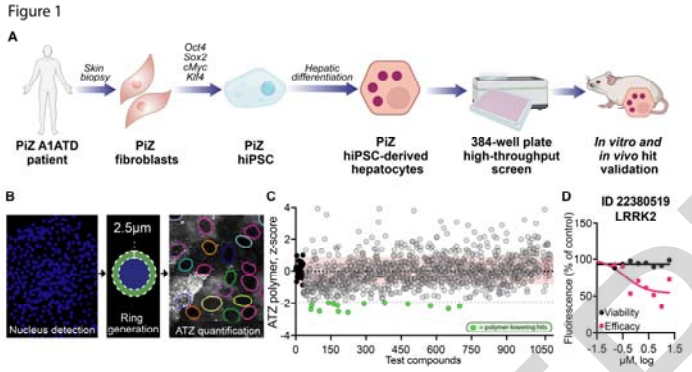

Figure 2: Validation of a range of LRRK2 inhibitors in iPSC-hepatocytes and ATZ CHO-K1 cell line.

(A) Representative confocal images showing polymeric ATZ expression (green) in patient-derived iPSC- hepatocytes treated with same panel of LRRK2 inhibitors (10μM) as indicated. Scale bar, 150μm. (B) Treatment of PiZ patient-derived iPSC-hepatocytes with LRRK2 inhibitor panel demonstrates significant reduction of polymer (2C1) (left) following 48h treatment without reducing cell number (viability) (right). Data normalised to vehicle control. Each dot represents a biological replicate. (C) The effects of LRRK2 inhibitors are conserved in Tetracycline-inducible (Tet-ON) CHO-K1 cells and demonstrate dose-dependent polymer reduction (pink curve, inhibition) and viability (black curve, cytotoxicity) following 48 hours treatment. N=3. Nonlinear regression by four-parameter curve fit. Statistical analysis by ordinary ANOVA test followed by Dunnett's multiple comparison test against the control. Data are represented as mean ± SD. *p<0.05, **p<0.01, ***p<0.001, ****p<0.0001.

Figure 1

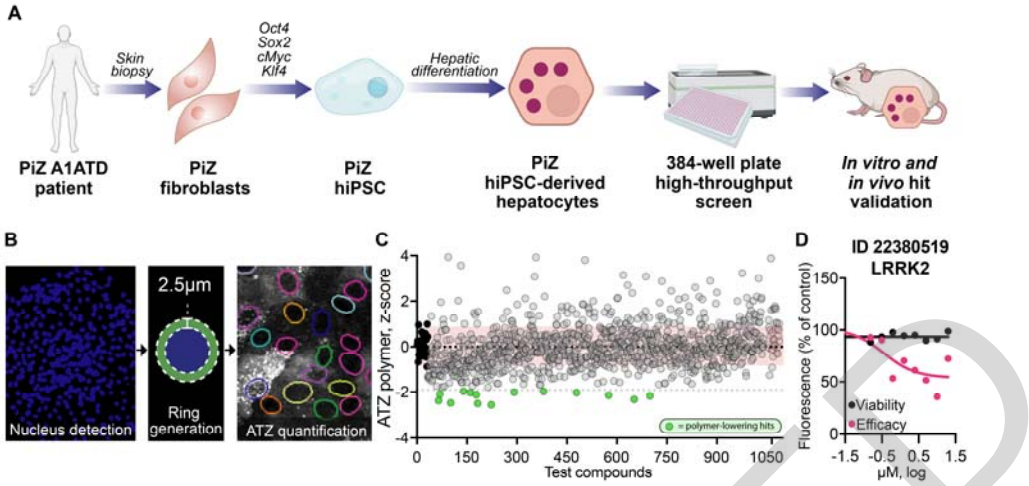

(B)

Figure 3: CZC-25146 reduces ATZ polymer and restores AAT secretion *in vitro*, without compromising cell viability. (A) Representative immunofluorescence images demonstrating ATZ polymer reduction in PiZ patient-derived iPSC-hepatocytes (middle row, green) with preserved total AAT (top row, red) after 24-hour treatment with CZC-25146 (middle column) compared to vehicle (left column) and healthy donor (right column) controls. Scale bar, 100µm. (B) Dose-dependent effects of CZC-25146 on polymer load (top graph), cell count (middle graph), and viability (bottom graph) over 24 hours, tested in three distinct PiZ patient iPSC lines. (C) CZC-25146 at varying doses (high: purple bars, low: green bars) decreases intracellular ATZ polymer versus untreated (grey bars) and vehicle controls (pink bars), with (D) non-significant impact on total intracellular AAT levels. N=5-10. (E) Immunoblot of soluble and insoluble intracellular immunoprecipitated ATZ polymer fractions. CZC-25146 treatment reduces both ATZ polymer fractions in PiZ iPSC-hepatocytes. Values normalised to the total signal (sum) of insoluble and soluble fractions in the vehicle control group. N=8. (F) CZC-25146 significantly enhances AAT secretion. N=8. Statistical analysis by Kruskal-Wallis test, followed by a Dunn's multiple comparison test. Data are represented as mean ± SD. *p<0.05, **p<0.01, ***p<0.001, ****p<0.0001. Veh = vehicle.

Figure 3

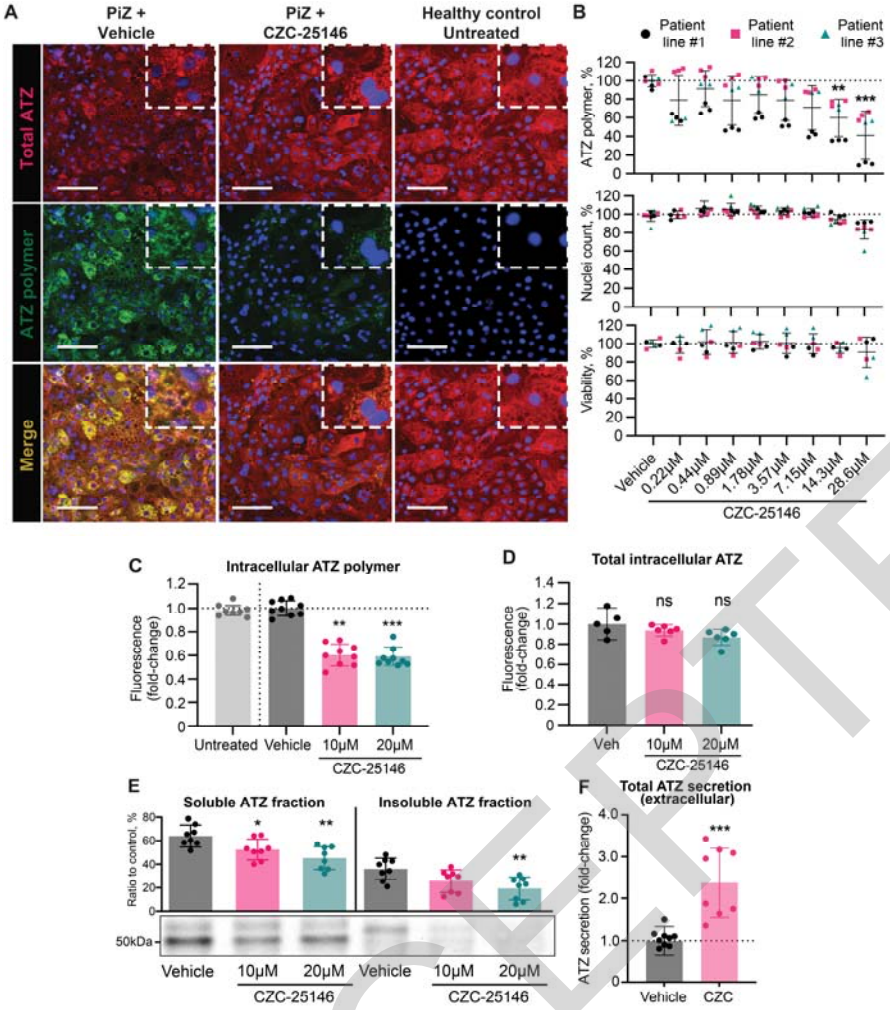

Figure 4: CZC-25146 reduces ATZ polymer and decreases inflammation in the PiZ mouse liver. (A) Representative images of polymer load (PASD staining) in PiZ mouse livers following treatment with CZC-25146 (CZC, middle) or vehicle control DMSO (left). Healthy C57BL/6 mouse liver (right) shown as control. LL = left lateral lobe, LM = left medial lobe, CL = caudate lobe, RM = right medial lobe, RL = right lateral lobe. Scale bar, 150μm. (B) Quantification of staining from a showing reduction in each of the five liver lobules (top) and in aggregate (bottom) following treatment with CZC-25146 (pink bar), vehicle control (grey bar) or with no treatment (purple bar). (C) Immunoblot of immunoprecipitated ATZ demonstrates a significant decrease of polymers in the livers of PiZ mice treated with CZC-25146. (D) Serum levels of total human alpha-1 antitrypsin in PiZ mice treated with CZC-25146 show significant increase compared to wildtype mice and vehicle group (DMSO). (E) Serum levels of the polymeric ATZ in the mouse serum showed a significant increase in CZC-treated mice compared to vehicle group (DMSO). (F) Levels of inflammatory cytokines in liver tissue were reduced in animals treated with CZC (pink bar) compared to vehicle control (grey bar) returning to levels seen in the no treatment (green bar) group. N=5 mice per group. (G) RT-qPCR shows CZC-25146 treatment has no impact on the LRRK2 gene expression of PiZ liver. (H) Representative images (left) and quantitative assessment (right) of immunoblotting analysis on the extracted protein from the liver of the PiZ mice treated with CZC-25146 compared to vehicle only and untreated (WT - healthy mouse) controls showing significant reduction in LRRK2 activity as shown by the LRRK2 phosphorylation status (pSer935-LRRK2) compared to the vehicle only control. Statistical analysis by unpaired Student t-test. N=3 mice. Data are represented as mean ± SD. *p<0.05, **p<0.01, ***p<0.001, ****p<0.0001.

Figure 4

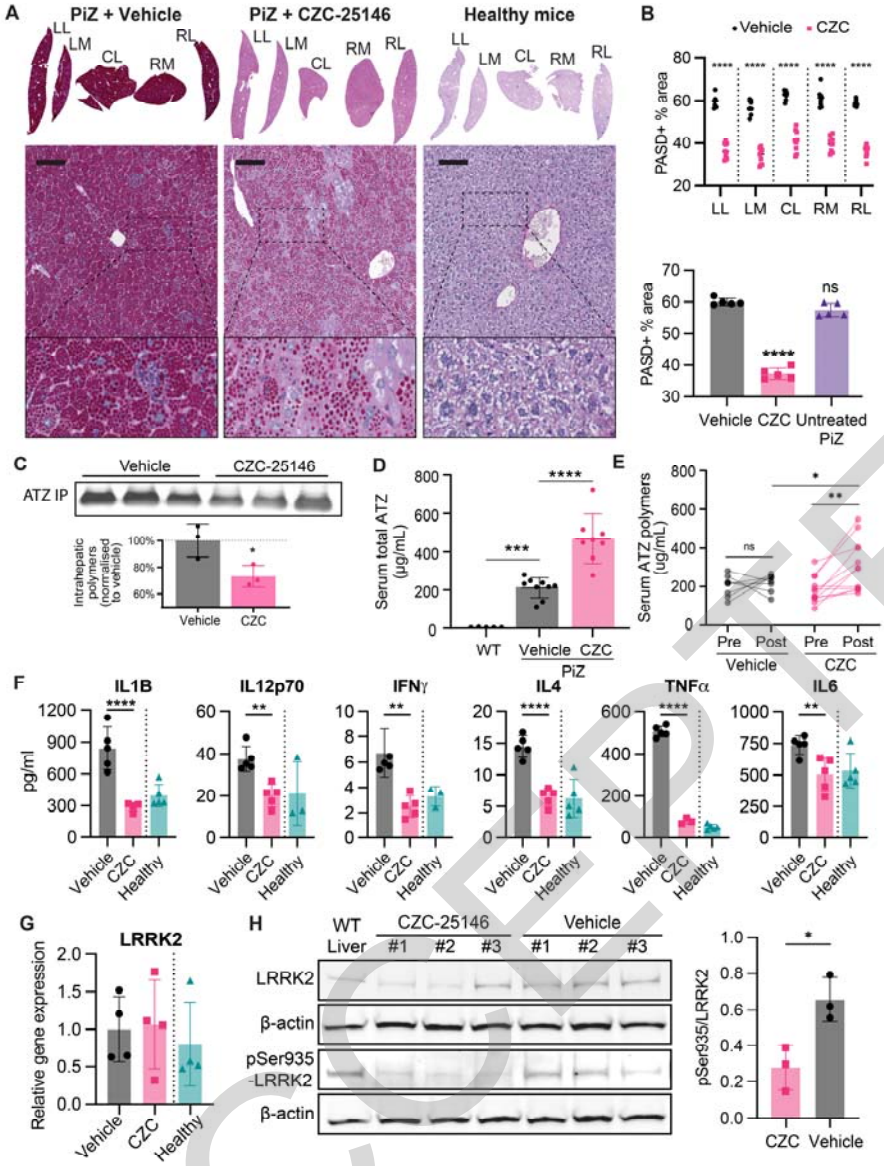

Figure 5: CZC-25146 reduces ATZ polymerisation in ATZ in CHO-ATZ model. (A) CHO-K1 Tet-On cells expressing ATZ were induced with doxycycline (0.5 µg/ml) for 48h and incubated with 10µM CZC-25146 or 0.1% v/v DMSO during the induction. Cells were then labelled with 35S Met/Cys and chased at the indicated times. Culture media were collected, and cells were lysed in 1% v/v NP-40 buffer. Intracellular fractions and culture media from cells expressing ATZ were immunoprecipitated first using polymer-specific 2C1 monoclonal antibody and then with anti-human polyclonal antibody. Samples were resolved by 4–12% w/v acrylamide SDS–PAGE and detected using autoradiography. White and black arrowheads indicate the complex and high-mannose glycosylated forms of AAT, respectively. (B) Autoradiograms from two independent experiments were quantified by densitometry to determine AAT levels, using the Image Studio Lite software (LI-COR Biosciences, Cambridge, UK). Graphs show mean ± standard error of the mean of radioactive AAT normalized to the t = 0 sample for each variant (n = 2). Statistical analysis by multiple unpaired Student T-tests. N=2. *p<0.05, **p<0.01, ***p<0.001, ****p<0.0001.

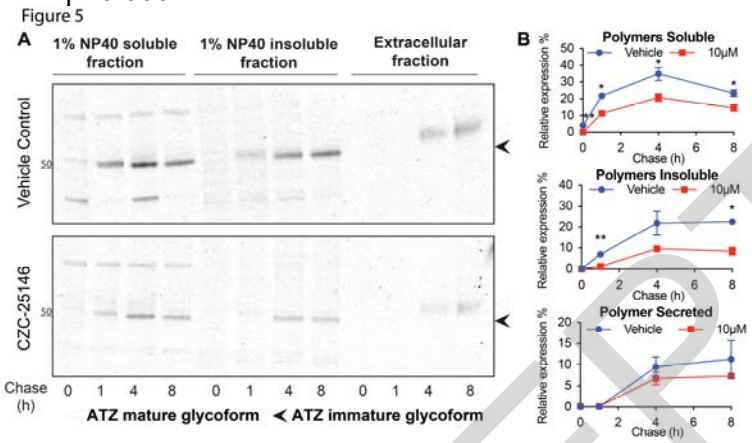

Figure 6: CZC-24156 induces autophagy *in vitro* and *in vivo*. (A) Representative images of LC3-GFP fibroblasts, following treatment with CZC-25146 (CZC, middle), vehicle control (left) or positive control Rapamycin (right). Images taken 2 hours after exposure. Scale bar, 50µm. (B) Time course analysis following CZC (pink), or Rapamycin (green) treatment shows significant upregulation of LC3 expression from 2-10 hours compared to vehicle controls (grey). (C) RT-qPCR shows dose responsive increased expression of genes involved in the autophagy pathway following addition of CZC to patient-derived iPSC-hepatocytes at Low (pink) = 14.3µM or High (green) = 28.6µM concentrations. N=4 replicates. (D) Representative immunoblotting images (left) and quantification (right) of LC3 isoforms from PiZ patient iPSC-hepatocytes following treatment with CZC-25146 (CZC, middle), vehicle control (left) or positive control Rapamycin (right). N=3. (E) Autophagic flux assay demonstrating the induction of autophagic degradation in PiZ iPSC-hepatocytes by CZC-25146. This is demonstrated by an increase in LC3-II expression in response to escalating doses of CZC-25146 alone (left), and a further accumulation of LC3-II when cells are treated with CZC-25146 in conjunction with Bafilomycin A (right). (F) Representative images (left) and semi-quantitative analysis (right) showing the effect of treatment with CZC alone (left middle), CZC + autophagy inhibitor, NH_4Cl (right middle), NH_4Cl alone (far-right) or vehicle control (far left) on ATZ polymer (2C1 expression, green) in patient-derived iPSC-hepatocytes. Scale bar, 100µm. (G) Representative macroscopic (top) or zoomed in (bottom) images of LC3 staining in livers of PiZ (far left), healthy mice (far right), CZC-25146 treated (right middle) or vehicle control (left middle). (H) Quantification of images from (G) separately analysed by each liver lobe (left) or pooled (right). Quantification was conducted using ImageJ. N=5 mice per group. Statistical analysis by Ordinary ANOVA test, followed by Dunnet's multiple comparisons test. Data are represented as mean ± SD. *p<0.05, **p<0.01, ***p<0.001, ****p<0.0001.

Figure 6